Geophysical Journal International

Geophys. J. Int. (2011) **184,** 689–698 doi: 10.1111/j.1365-246X.2010.04887.x

Broad-band waveforms and robust processing for marine CSEM surveys

David Myer, Steven Constable and Kerry Key

Scripps Institution of Oceanography, IGPP, La Jolla, CA 92093-0225*, USA. E-mail: dmyer@ucsd.edu*

Accepted 2010 November 8. Received 2010 October 13; in original form 2010 July 14

SUMMARY

In the marine controlled-source electromagnetic method, the Earth response varies in frequency; therefore, using a wide range of frequencies may better constrain geological structure than using a single frequency or only a few closely spaced frequencies. Binary waveforms, such as the square wave, provide a number of frequencies, though many are limited in usefulness because of the rapid decline of amplitude with frequency. Binary waveform design can be improved by recognizing that the class of doubly symmetric waveforms has special properties: they are compact, have controlled phase, are never polarizing and can be described by a simple closed-form mathematical solution. Using this solution, we discovered a compact waveform in which the amplitudes of the third and seventh harmonics are maximized and which has a signal-to-noise advantage at higher frequencies over several other common waveforms.

Compact waveforms make possible improved methods for time-series processing. Using short time windows and a first-difference pre-whitener lessens spectral contamination from magnetotelluric signal and oceanographic noise; robust stacking reduces bias from time-series noise transients; and accurate variance estimates may be derived from averages of waveform-length Fourier transform windows of the time-series.

Key words: Time-series analysis; Fourier analysis; Marine electromagnetics.

1 INTRODUCTION

In the frequency domain marine controlled-source electromagnetic (CSEM) method, an electromagnetic dipole is used to create a source field that is measured at receivers placed across the seabed (Cox *et al.* 1986; Constable & Cox 1996; MacGregor *et al.* 2001; Edwards 2005). This source dipole field couples with surrounding materials and the measured field is treated as a linear convolution of the source with an attenuative, diffusive earth (Ward & Hohmann 1987; Loseth *et al.* 2006). The frequency response of the Earth transfer function (TF) varies according to conductivity, source–receiver range and a variety of other (chiefly geometric) factors, with the result that the CSEM method is sensitive to thin resistive bodies embedded in conductive sediments. This has led to its increasing use in hydrocarbon and gas-hydrate exploration (e.g. Eidesmo *et al.* 2002; Ellingsrud *et al.* 2002; Weitemeyer *et al.* 2006; Constable & Srnka 2007).

Because the peak frequency sensitivity of an exploration target is not well known *a priori*, it is common to transmit a source waveform, which allows for simultaneous broadcast of multiple frequencies. The classic example of such a waveform is the square wave, which provides a spread of frequencies at the odd harmonics of the fundamental transmission frequency. However, the square wave is not ideal for the CSEM method because the amplitude of its harmonics falls off as $1/n$, where n is the harmonic number. For an inductive method like CSEM in which fields attenuate exponentially as a function of range and frequency, many of the square wave's harmonics have too little power to be detected to useful ranges.

The signal-to-noise ratio (SNR) of the measured CSEM signal is directly related to the source dipole moment (SDM) of the transmitter. Since the SDM is composed of three factors, this suggests that there are three modifications to a transmitter, which may increase the SNR: increase the output current, lengthen the transmitter dipole and modify the waveform. Existing transmitters output up to 1000 amps. Increasing this value is technically difficult, increases the danger and complexity of ship-board operations and may eventually run into environmental concerns. Transmitter dipole lengths up to 300 m are common, but because of the complexity of deep-towing a streaming antenna near the seabed, longer dipoles are impractical. In contrast, customizing the waveform is a relatively easy way to increase the SDM at particular frequencies.

Specialized waveforms have been presented by Constable & Cox (1996) and patented by ExxonMobil (Lu & Srnka 2005). Mittet & Schaug-Pettersen (2008) present a collection of waveforms discovered using a Monte Carlo approach for finding waveforms that fit a given criterion. In this paper, we discuss classes of waveforms, develop an analytical method for finding the optimal second-order symmetric waveform for any given criterion and compare the bandwidth of an example waveform so derived with those mentioned above. We also discuss techniques for time-series processing which take advantage of compact waveforms to reduce

spectral contamination and provide accurate variance estimates. We show examples from a recent academic CSEM survey over a gas prospect on the northwestern Australian shelf.

2 WAVEFORM CLASSES

CSEM waveforms are usually either binary (alternating polarity between constant positive and negative output current) or ternary (positive and negative separated by 'off' states). Ternary waveforms are sometimes intentional (e.g. Constable & Cox 1996) and sometimes required due to hardware limitations (e.g. Sinha *et al.* 1990; Mittet & Schaug-Pettersen 2008). Regardless of the reason, we note that introducing time in a waveform in which the transmitter is off decreases the integrated output current and therefore the cumulative SNR. Thus we primarily consider binary waveforms in this work. However, the mathematical development presented here applies equally well to ternary waveforms with one small addition, which we note after the main development.

The family of binary waveforms may be divided into three classes based on symmetry: asymmetric, singly symmetric and doubly symmetric. In a singly symmetric waveform, the second half of the waveform is either the mirror image of the first half or the mirror image with reversed polarity. (Note that to avoid confusion we refer to these as 'mirror' and 'rotational' symmetry, respectively, and restrict the use of the classical terms 'even' and 'odd' to the discussion of harmonic numbers.) In a doubly symmetric waveform, each half of the waveform is itself composed of two symmetric halves. For the waveform to be doubly symmetric, the quarter symmetry must be opposite in sense to the half symmetry; that is, if the waveform is rotationally symmetric about its centre, then the quarters must have mirror symmetry. The square wave is an example of a doubly symmetric waveform with rotational half symmetry and mirror quarter symmetry. Fig. 1 shows examples of the three classes. Note that doubly symmetric waveforms are constructed of an asymmetric segment which is repeated four times with alternating symmetry: rotational, mirror, rotational; or mirror, rotational, mirror. The slight change in ordering corresponds to a 90° shift of the waveform as is shown in plots (d) and (e) of Fig. 1.

To evaluate the usefulness of a particular class of waveforms for CSEM and other frequency domain exploration techniques, we examine the familiar Fourier series expansion given by eqs (1) to (4).

$$f(t) = a_0 + \sum_{n=1}^{\infty} a_n \cos(2\pi nt/T) + \sum_{n=1}^{\infty} b_n \sin(2\pi nt/T), \tag{1}$$

where

$$a_0 = \frac{1}{T}\int_{-T/2}^{T/2} f(t)\,\mathrm{d}t, \tag{2}$$

$$a_n = \frac{2}{T}\int_{-T/2}^{T/2} f(t)\cos(2\pi nt/T)\,\mathrm{d}t, \tag{3}$$

$$b_n = \frac{2}{T}\int_{-T/2}^{T/2} f(t)\sin(2\pi nt/T)\,\mathrm{d}t. \tag{4}$$

Here $f(t)$ is the time domain representation of a waveform, T is the time length of one full wave, t is time and n is the harmonic number. Eq. (1) is a statement of the Fourier theorem, namely that any waveform can be decomposed into parts with mirror and rotational symmetry about $t = 0$. Eq. (2) is the mean of the waveform (i.e. its DC component). Eqs (3) and (4) are the frequency domain amplitude coefficients of the nth harmonics and correspond, respectively, to sinusoidal components with mirror symmetry about $t = 0$ and rotational symmetry about $t = 0$.

Eq. (2) is zero unless the waveform has a non-zero mean. In practice, a non-zero mean has several undesirable side effects, which should be avoided. First, it indicates a polarizing waveform which, in a marine environment, accelerates the destruction of the current carrying electrodes through ablation. Secondly, a non-zero mean indicates that some of the total power of the waveform is in the DC component. Since total power is finite and conserved, a non-zero DC component indicates that the frequency domain components have less overall power and thus lower SNR. Though one might surmise that the non-zero mean produced by a polarizing waveform could be useful as a proxy for DC measurements, it will be confounded by various sources of self-potential across the receiver electrodes and, therefore, likely useless.

In eqs (3) and (4), when $f(t)$ has rotationally symmetric halves $a_n = 0$, and when $f(t)$ has mirror symmetric halves $b_n = 0$, for all n. If the waveform is doubly symmetric, the even values of n cancel, leaving only odd harmonics (as is the case for the square wave).

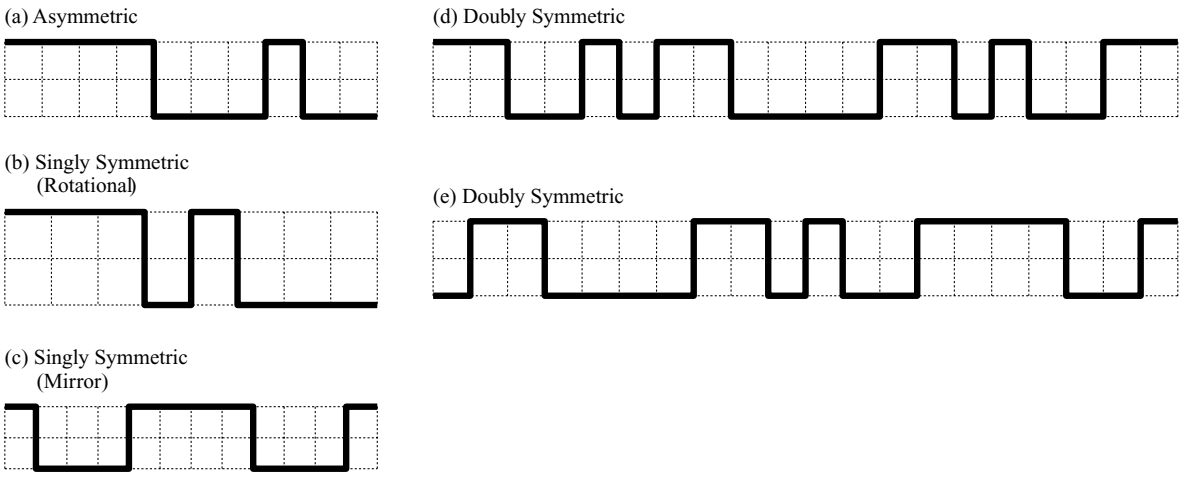

Figure 1. Examples of the three classes of waveforms: (a) asymmetric, (b) singly symmetric with rotational symmetry, (c) singly symmetric with mirror symmetry and (d) and (e) doubly symmetric. Note that waveform (e) is merely waveform (d) shifted 90°. This is the waveform currently in use by our group.

When $f(t)$ is binary or ternary, the integrals in eqs (3) and (4) are trivial to solve because $f(t)$ has only the values -1, 1 or 0. Eq. (3) becomes a sum of sine terms and eq. (4) a sum of cosine terms. The coefficients a_n and b_n interact through the oscillatory terms in eq. (1) to determine the amplitude and phase of the frequency domain harmonics of the waveform. Thus when either a_n or b_n is zero, the output phase will be 0, 90, 180 or 270 degrees.

For an asymmetric waveform, eqs (2)–(4) may all be non-zero, yielding both even and odd harmonics of a variety of magnitudes and phases and in some cases a polarizing non-zero mean. This forms the largest class of waveforms and includes many subclasses such as: pseudo-random binary sequences, which attempt to provide a white signal spectrum; chirps, which sweep through a range of frequencies; and sequential waveforms, in which multiple waveforms of different fundamental frequencies are transmitted sequentially. We experimented with sequential waveforms and found them to produce overly complicated data with the inductive decay from one fundamental frequency contaminating the time-series of the next fundamental. Users of any waveform searching technique will want to discard a large number of sequential and polarizing waveforms in the search for a solution.

Singly symmetric waveforms have either non-zero a_n or non-zero b_n for all n, so the phase of each harmonic is a well-controlled multiple of $\pi/2$. Even and odd harmonics may both exist, giving densely spaced frequencies. However, some mirror symmetric waveforms are polarizing.

Doubly symmetric waveforms also have either non-zero a_n or b_n for all n, but due to cancellation are limited to odd harmonics only. They have the desirable quality that it is impossible for doubly symmetric waveforms to be polarizing since they are constructed from a short time segment that is repeated twice in each polarity. Further, they have a discrete mathematical form which makes it simple to search all possible waveforms to find the one which best fits a given set of criteria.

3 FINDING THE OPTIMAL WAVEFORM

To develop the mathematical form we need, we begin with the simple, doubly symmetric waveform in Fig. 2. This waveform has rotational symmetry in the centre, so all a_n are zero. The solution of eq. (4) is given by

$$b_n = \frac{4}{\pi n}\left[\frac{1}{2}\cos\left(2\pi n\frac{4}{8}\right) - \cos\left(2\pi n\frac{3}{8}\right) + \cos\left(2\pi n\frac{1}{8}\right) - \frac{1}{2}\right], \tag{5}$$

where we have not simplified the fractions introduced by t to emphasize that each term comes from a specific polarity transition in the waveform. Because $\cos(-t) = \cos(t)$ and the sign of the polarity change at t is the same as at $-t$, cosine terms from the latter half of the waveform reinforce those in the former half. Thus the equation contains four terms: one for the end, one for the middle and one for each transition inside the half waveform. This pattern holds true

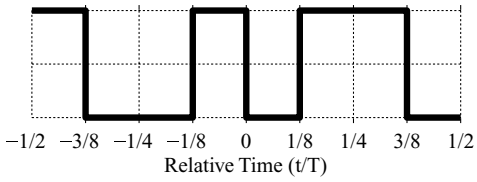

Figure 2. Simple, doubly symmetric waveform with rotational symmetry in the centre and mirror symmetry at the quarters. Its Fourier coefficients are given by eq. (5).

for any doubly symmetric waveform with rotationally symmetric halves. The expansion for the waveform in Fig. 1(e), for example, has six terms because there are four transitions in the half wave. The expansion of the standard square wave has only the terms for the end and the centre because there are no transitions in the half wave. Note in eq. (5) that when n is even, the terms interfere destructively in pairs, effectively eliminating all even harmonics. If there were an odd number of transitions in the half wave, then a term would be left unpaired and there would be even harmonics. However, in a doubly symmetric waveform, the repetition of the quarter wave ensures that there are always an even number of transitions and thus only odd harmonics.

A pattern similar to eq. (5) can be derived from eq. (3) in doubly symmetric waveforms with mirror symmetric halves. However, since a mere shift of 90° changes these to rotationally symmetric halves, we ignore this solution as trivially redundant.

We note that a ternary waveform has the same class of solutions as a binary waveform. The difference is that the off state during each polarity change splits every term in eq. (5) into two terms with half amplitudes. So, for example, $\cos(2\pi n\ 3/8)$ becomes $^1/_2\ \cos(2\pi n\ [3/8 - \delta]) + {}^1/_2\ \cos(2\pi n\ [3/8 + \delta])$, where δ is one half of the off time. The split cosine terms interact destructively, decreasing the amplitude at each frequency. When both n and δ are small, the difference between a ternary and binary waveform is small. However, as either n or δ increases, the decrease in amplitude becomes quite large and results in frequencies with very little usable range. Also, as δ increases, the SNR of the entire waveform decreases because the total output current is diminished. Thus, a binary waveform transmitter is preferred to a ternary waveform transmitter.

The importance of the example given in eq. (5) is that doubly symmetric waveforms have a simple mathematical form. When searching for new waveforms, there is no need to construct a time-series for each possibility and Fourier transform it to get the amplitude of the frequency components. Instead, the spectrum is determined by the time of each transition in the waveform. This suggests that a compact general form may be derived in which the number of cosine terms is a function of the number of transitions. However, we first note that singly symmetric waveforms have the same solution form as the example in eq. (5). Because single symmetry allows polarized waveforms, we must take an additional step to exclude them from our solution set. This is easily solved by recognizing that in double symmetry the transition times in the second quarter of the waveform are a function of the times in the first quarter. Thus we have a general solution, which is parametrized in terms of the number and times of the polarity transitions in the first quarter of the waveform.

$$b_n = \frac{4}{\pi n}\left[\frac{1}{2}\cos(\pi n) - \frac{1}{2} + \sum_{j=1}^{\tau}(-1)^j\left[\cos(2\pi n t_j) - \cos\left(2\pi n\left\{\frac{T}{2} + t_j\right\}\right)\right]\right], \tag{6}$$

where T is the total length of the waveform in time, τ is the number of transitions in the first quarter, and t_j is the time of each transition in that quarter expressed as a function of T.

While transitions can theoretically be placed infinitely close to one another, in reality, digitally controlled hardware involved in both the transmitter and receiver imposes limitations on switching and sampling rates. Most importantly, the waveform transitions are discretized by the switching frequency of the transmitter. Our present transmitter, for example, runs at 400 Hz, so any waveform it produces must have polarity transitions which are an integer multiple

Table 1. The harmonic amplitudes and phases of the doubly symmetric waveform shown in Fig. 1(d) and compared with other commonly used waveforms in Figs 3 and 4. Only harmonics with an amplitude >0.10 are shown.

Harmonic number	Amplitude	Phase	Harmonic number	Amplitude	Phase
1	0.35	0	13	0.40	0
3	0.88	0	17	0.16	180
5	0.25	0	23	0.12	0
7	0.74	180	27	0.19	180
9	0.24	0	33	0.16	0
11	0.20	180	47	0.11	180

of 2.5 ms apart. Further, to be robustly sampled, a waveform must have transitions that are far enough apart in time (the 'minimum time') that they meet certain criteria. First, the minimum time must be long enough to allow the transmitter to reach full output power after switching. This time is highly dependent on the electronic components of the transmitter and the inductance of the antenna and must be experimentally determined. Secondly, according to the sampling theorem, the minimum time must be long enough to allow the receiver to sample a transition.

With these limitations, the number of possible waveforms decreases from infinity to a reasonable number. For example, for a 1 s waveform, a transmitter able to switch at 400 Hz, a receiver sampling at 50 Hz and requiring a minimum of two receiver samples of minimum time, there are 60331 possible doubly symmetric waveforms. A simple MATLAB program using eq. (6) to inspect every possible waveform for one that matches a given criterion (e.g. the highest amplitude of the sum of the third & seventh harmonics) takes about 12 s on an ordinary laptop.

There are cases where there are too many possible waveforms to make searching the entire set practical. (e.g. for an 8 s waveform with the same criteria as above, there are well over 10^{17} doubly symmetric waveforms!) In this situation, it is advisable to combine our analytic formulation with a stochastic search method such as Monte Carlo to find a suitable waveform in a reasonable amount of time. While such a method cannot be said to find the one optimal waveform fitting the criterion, it may certainly find one suitable for exploration purposes.

4 THE WAVEFORM IN PRACTICE

Since in the CSEM method higher frequencies attenuate more rapidly and are limited to sensing shallower structure, choice of frequency is important. Model studies of 1-D synthetic data show that having two widely spaced frequencies improves the resolution of inversion results (Key 2009). Key also shows that for synthetic modelling, there is no benefit to having a dense collection of frequencies because the Earth TF varies smoothly in frequency. We note, however, that while a forward model of a target survey area may identify a preferred frequency, unexpected geological conditions may interfere and shift the peak response. There may also be enough uncertainty regarding the Earth structure to be explored that an optimal frequency cannot be determined *a priori*. Additionally, noise encountered in the marine environment is commonly band limited and may adversely affect one or more target frequencies. It is often difficult to predict the frequency of such noise ahead of time, so having a broad spectrum of frequencies is desirable to mitigate these effects. While using a square wave provides one decade of frequencies with harmonic amplitudes above 10 per cent of the peak current, most of the signal is concentrated in the fundamental with the next frequency available (the third harmonic) at only 42 per cent amplitude.

We used the process described in the preceding section to search for a waveform with maximum amplitude in the third and seventh harmonics. Setting the target frequency as the third harmonic rather than the fundamental allows for the lowest frequency to establish background structure or to provide a safeguard if the estimated optimal frequency is too high. Also, increasing power in the seventh harmonic ensures higher amplitude across at least one half decade of frequency.

We discovered the waveform shown in Fig. 1(d) (hereinafter referred to as 'D') and whose output amplitudes are listed in Table 1. In Fig. 3(a), we compare waveform D to a square wave. The amplitude of the fundamental is 0.35, which is low. However, the power has been spread to higher frequencies so that the $1/n$ fall-off observed in the higher harmonics of the square wave is mimicked but at higher amplitude. The highest harmonic above 10 per cent amplitude is the 47th harmonic and the total spread of frequencies above 10 per cent covers nearly two decades.

Fig. 3(b) compares waveform D with the doubly symmetric ternary waveform presented by Constable & Cox (1996) (hereinafter referred to as 'Cox'). The Cox waveform has amplitude concentrated in the first and third harmonics with each at about 78 per cent. Most other harmonics are low, with total coverage

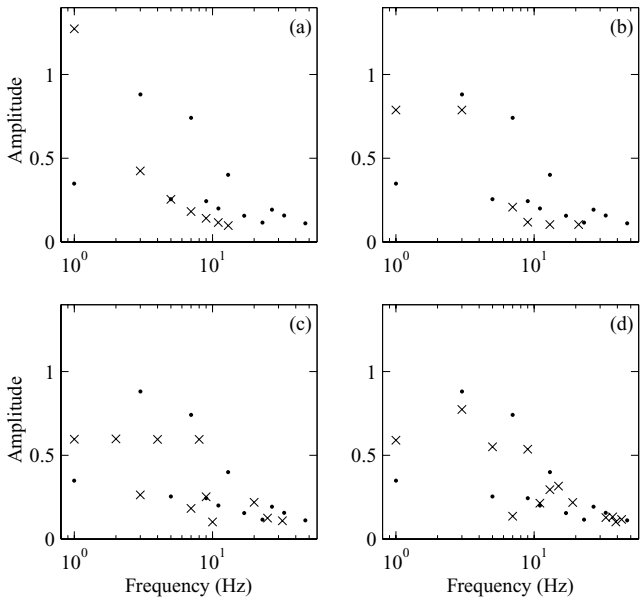

Figure 3. Comparison of the amplitudes of the waveform D (filled circles) with several other waveforms in use (crosses). Frequencies whose amplitudes are below 0.1 of peak current have been excluded. Comparison waveforms are from (a) a square wave, (b) the Cox waveform, (c) the LS waveform and (d) the MSP waveform. The x-axis is $\log_{10}$ frequency. The fundamental for each waveform is set to 1 Hz and the peak output current to 1.0. All harmonics are odd integers with the exception of the LS waveform, which is asymmetric and thus has some even harmonics.

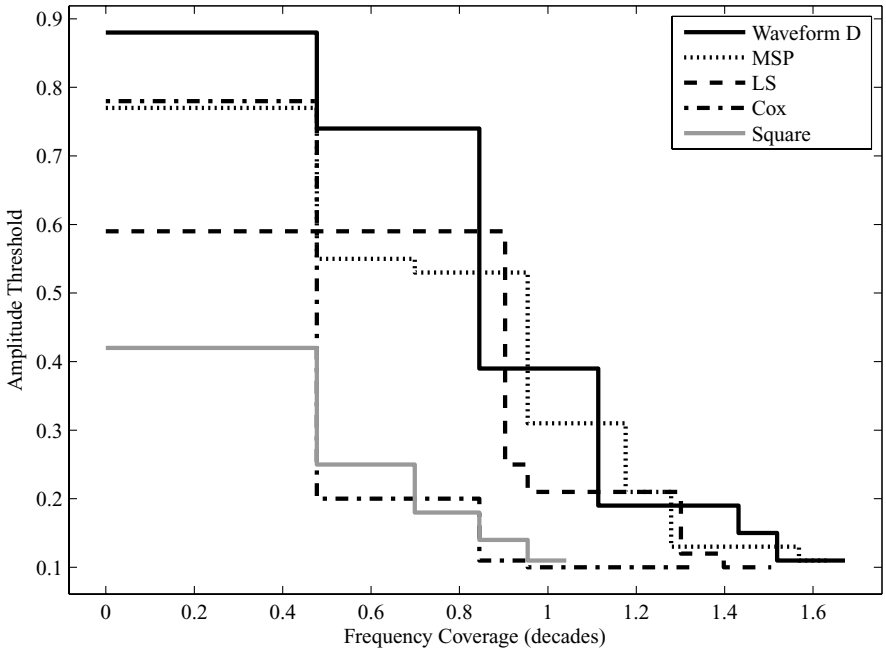

Figure 4. Plot of amplitude threshold versus frequency coverage for the waveforms compared in Fig. 3. For a given output amplitude threshold, the plot shows the number of decades of frequency between the fundamental and the highest harmonic above the threshold. The D and MSP waveforms have similarly broad frequency coverage, though waveform D has an advantage in the first decade. Total coverage is ∼1.7 decades at an amplitude threshold of 0.1 (i.e. 10 per cent output amplitude).

above 10 per cent just passing a decade in frequency. We note that for this ternary waveform the output current is off for 31 per cent of the time, significantly reducing the SNR of all frequencies when compared with a binary waveform with the same peak-to-peak output current.

ExxonMobil have patented several waveforms with equal power in a series of pseudo-logarithmically spaced frequencies covering one decade (Lu & Srnka 2005). These are asymmetric, polarizing waveforms. However, for comparison we show in Fig. 3(c) the waveform with the broadest frequency range for which timing is provided in the patent filing (hereinafter referred to as 'LS'). The LS waveform was designed to mimic a pseudo-random binary sequence in which the output amplitude is approximately 60 per cent for the first, second, fourth and eighth harmonics. Because it is an asymmetric waveform, it has both even and odd harmonics and the total output power, which is conserved, is divided among more harmonics than a symmetric waveform. Many harmonics have close to zero amplitude and those above the eighth harmonic fall off rapidly. Nevertheless, the total frequency coverage above 10 per cent is almost 1.5 decades.

Mittet & Schaug-Pettersen (2008) presented three waveforms of which we compare the one with the broadest frequency range (hereinafter referred to as 'MSP') in Fig. 3(d). Since timings are not provided in their paper, we have approximated the waveform from their Fig. 4. The amplitudes of the first, fifth and ninth harmonics are almost 60 per cent while the third harmonic is about 70 per cent. Higher harmonics fall off at a rate similar to waveform D.

Fig. 4 is a comparison of the frequency coverage of the five waveforms discussed above. For each waveform, we plot the frequency coverage between the fundamental and the highest harmonic above a given output amplitude threshold, where the frequency coverage is defined as the difference of the $\log_{10}$ harmonic frequency and fundamental frequency. For example, for the Cox waveform, there is a little less than half a decade of frequency coverage provided by harmonics above a 0.3 amplitude threshold. Note that we use the fundamental as the low end of the frequency band regardless of its amplitude because it has a large skin depth compared to the harmonics and therefore the longest range detection, even when its amplitude is suppressed. Through the whole range of cut-off thresholds, waveforms D and MSP perform similarly. However, waveform D has a slight SNR advantage in the first decade.

In the waveforms shown in Figs 3 and 4, some effort has been made by the various authors to retain output power in the fundamental frequency; whereas we placed no constraint on the fundamental, sacrificing its amplitude for enhanced higher harmonics. We believe that this approach is beneficial for three reasons. First, lower frequencies have lower attenuation, thus propagating farther than higher frequencies even at reduced transmission amplitudes, so higher amplitude is not necessary. Secondly, one may want to scale the waveform so that the peak amplitude harmonic is the frequency that is most sensitive to the target structure, and yet still be able to bracket it with frequencies on both the high and low sides. Having at least one lower frequency provides either data to help resolve background structure or insurance in case the target frequency turns out to have been set too high. Finally, because output power is conserved, decreased amplitude in the fundamental is associated with elevated amplitudes in higher harmonics. Waveforms like those shown in Fig. 3, in which the amplitude of the fundamental is kept high, may be decreasing the effective range of the higher frequencies.

We have now used waveform D in three large surveys: in 2008 in the Gulf of Mexico to study hydrates (Weitemeyer & Constable 2010), in 2009 off the coast of Australia to study the Scarborough hydrocarbon reservoir (Myer *et al.* 2010) and in 2010 off the coast of Nicaragua to study a subduction zone. We have usually selected a fundamental of 0.25 Hz. Fig. 5 is a plot of amplitude versus range from the Scarborough survey off the northwest shelf of Australia.

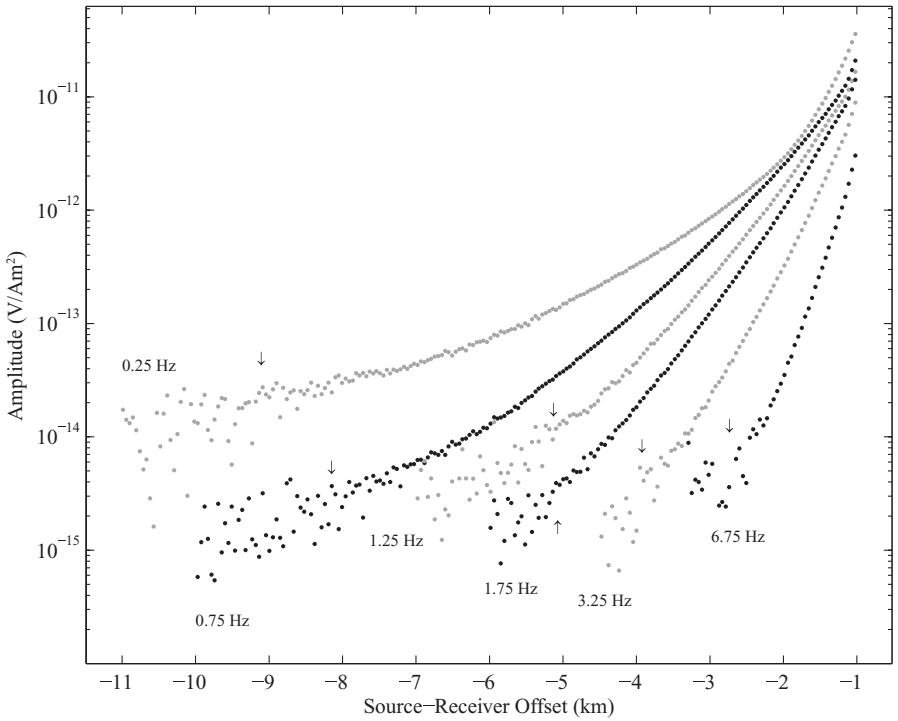

Figure 5. Inline horizontal electric field amplitude versus range data from a recent CSEM survey over the Scarborough hydrocarbon reservoir using waveform D. Arrows indicate the range at which each frequency's data reach SNR = 1. The augmented amplitude of the third harmonic (0.75 Hz) has raised its SNR sufficiently that it is detected to ranges that are within 1–2 km of the fundamental. Though the lower amplitude of the fundamental has limited its detection range, this does not adversely impact its usefulness in multifrequency inversion.

The survey is in 1 km of water with several kilometres of conductive sediments overlaying a resistive basement (a common hydrocarbon target scenario). From the amplitudes of the frequency components shown in Fig. 3(a), one might expect that the third harmonic, which has an amplitude of 0.88, should be detectable above the noise floor to farther ranges than the fundamental, whose amplitude is only 0.35. However, the data shown in Fig. 5 indicate that this is not the case. This is due to the complicated manner in which the SNR is affected by amplitude and frequency.

The maximum detection range for the electric field, which we define as the range at which the SNR declines to less than 1, is a function of the field's exponential decay rate. The decay rate is frequency dependent, such that higher frequencies approach the noise floor at a much steeper angle with increasing range than lower frequencies. Thus, even though changes in the amplitude of a source field frequency component affect its SNR linearly, the effect on maximum detection range is non-linear. As depicted in Fig. 5, raising the amplitude of the third harmonic raised its SNR sufficiently that it is detected to ranges that are within 1–2 km of the fundamental. Conversely, lowering the amplitude of the fundamental lowered its SNR and limited its detection range, though not adversely impacting its usefulness in multifrequency inversion. Evidently, waveform D has achieved a good balance between these two frequencies in a common hydrocarbon target scenario. We note, however, that the rate of electric field decay is also related to conductivity structure, and in a more resistive environment (e.g. sub-basalt hydrocarbon targets, mid-ocean ridges, etc.) the higher harmonics will also decay slowly. Explorers in these environments may find benefit in designing a new waveform, which augments harmonics that are over a decade above the fundamental. The mathematical process described in the previous section can easily accommodate this.

5 TIME-SERIES PROCESSING

Compact waveforms such as those discussed earlier lend themselves to particular statistical methods in processing. In the frequency domain CSEM method, the data of interest are not the time-series, but the TF estimates derived in the frequency domain. Workers in the CSEM method have not generally used the term 'transfer function' because they have focused on the change in amplitude and phase at one particular frequency over range. However, the CSEM response function also varies in frequency. With the growing use of multifrequency inversion, we prefer the term TF. In a typical TF estimate, the cross-spectrum of the input with the output signal is divided by the auto-spectrum of the input signal to derive the Earth system TF (Bendat & Piersol 2000, Ch. 6). Since the CSEM input signal is known, auto- and cross-spectral techniques are not necessary. Instead, the Fourier transform of the receiver time-series is simply divided by the complex Fourier components of the input signal (i.e. the output current measured at the transmitter). The result is then normalized by the source dipole length and corrected for the response function of the receiver. Because the whole process is linear, a number of statistical techniques may be applied to decrease spectral leakage, decrease the noise floor and derive a variance estimate for each complex TF.

In general, TF estimates are not necessary for very short time windows since the CSEM response varies smoothly in time. Typical transmitter tow velocities are on the order of 0.5–1.0 m s^{-1} (1–2 knots), so 1 min of time-series represents less than a typical antenna length. Though the movement of the transmitter means that the data are not statistically stationary, they are assumed to be so and it is common practice to apply a FFT to time-series windows that are one or more minutes long and ignore any bias which may be introduced (e.g. Behrens 2005). In Fig. 6, we quantify this bias using

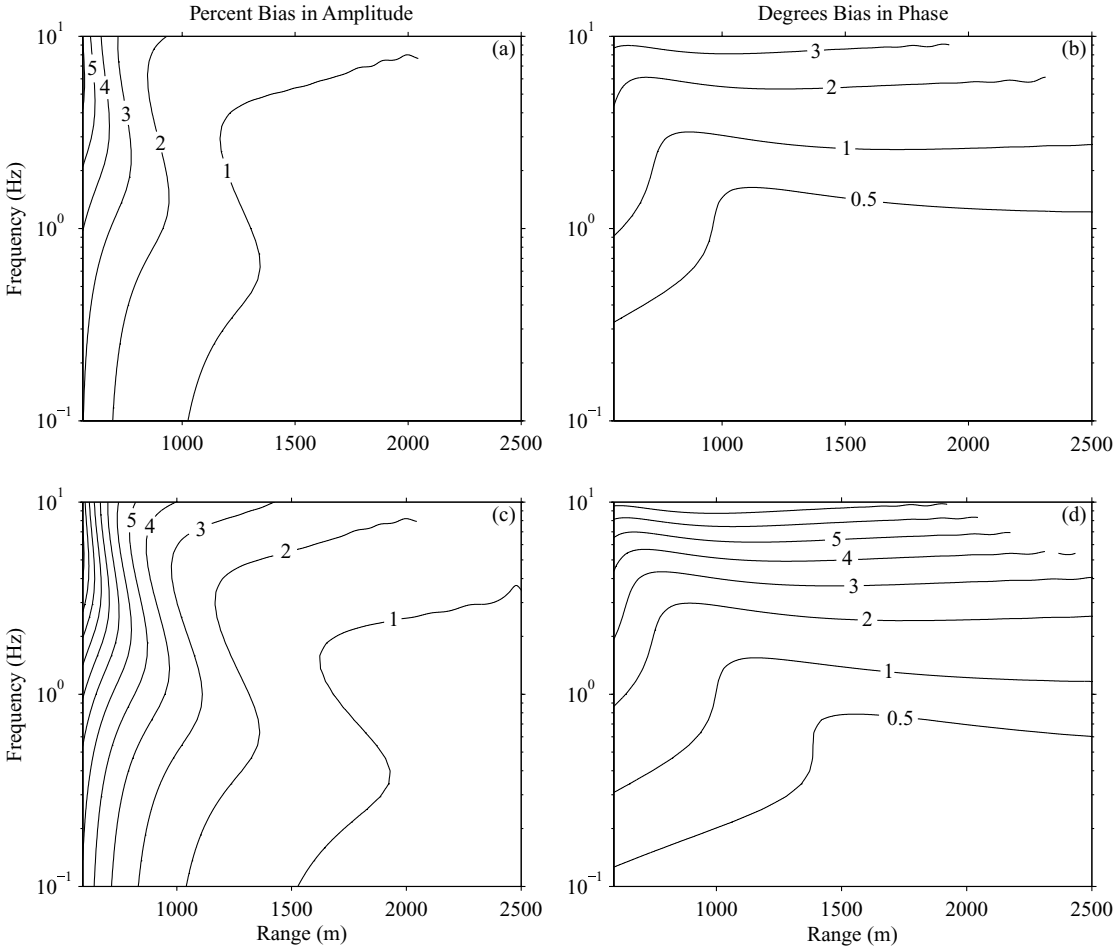

Figure 6. Percent bias in amplitude (a) and degrees bias in phase (b) due to non-stationarity of the CSEM source calculated for a 2-min stack length using a 1-D model described in the text. The amplitude bias decreases with range and increases with frequency as expected. The phase bias unexpectedly plateaus to a constant value for each frequency, indicating the complex nature in which the phase velocity is affected by the ocean–seafloor interface. Plots (c) and (d) are for a 3-min stack length and illustrate the increase in bias as stack length is increased.

a simple three-layer model and the 1-D CSEM modelling code of Key (2009), which we have modified to support a finite dipole source rather than a point dipole. The model is composed of a 1 km thick, 0.3 Ωm sea water layer between half-spaces of air (10^{12} Ωm) and sediment (1 Ωm). The transmitter is 50 m above the seafloor and is given a dipole length of 250 m. We calculate the inline response at receiver positions spaced at every metre between 500 and 2500 m for 31 frequencies between 0.1 and 10 Hz. Assuming a transmitter velocity of 1 m s^{-1}, these data points are also spaced every second in time. We used window lengths of 1–3 min and calculated the percentage bias by comparing the mean response of the complex field data within the time window to the response at the centre point of the window. Bias is a measure of the curvature in the data being stacked and is therefore primarily a function of the change in the field gradient.

The contours in Figs 6(a) and (b) are the percentage bias in amplitude and the bias in phase in degrees, respectively, for a 2-min stack length; (c) and (d) are for a 3-min stack length. The bias for the 1-min stack is insignificant (<1 per cent) for range >700 m and is not plotted. The bias increases with increasing stack window length, as expected. The rapid decline in amplitude bias with range reflects the exponential decay of the electric field and shows that even for the 3-min window length, the assumption of stationarity is reasonable after about 1500 m range. However, the bias in phase behaves quite differently than the bias in amplitude, levelling out to a minimum bias per frequency. The sharp turn in the phase bias contours is a strong function of the seafloor resistivity and the levelling of the bias contours is due to the phase velocity in the seafloor being modulated by energy leaking up from the seafloor into the water column. At much farther ranges, where the electric field from the air dominates, the phase velocity will become relatively constant and the phase stacking bias will reduce to zero.

Another problem with using a long time window is contamination by magnetotelluric (MT) signal. The MT signal is a broadbandwidth EM signal sourced in the ionosphere and impinging everywhere on the Earth. It has a red spectrum and while in a marine environment the higher frequencies can be attenuated by the overlying ocean, frequencies below 0.1 Hz are typically measurable. A 1-min FFT window in CSEM is subject to spectral leakage by MT signal, which contaminates the TF estimate (McFadden & Constable 1983). Additional similar sources of spectral leakage such as self-potential, electronic drift and motional inductance may also be present and minimized by the process described below.

First difference pre-whitening is a simple method to reduce spectral contamination that can take advantage of the compact waveform. Without a pre-whitener, the TF estimate for a long time window (e.g. 60 s) is identical to the average of TF estimates for short time windows covering the same time (e.g. fifteen 4 s windows)

when the signal is periodic, so there is no advantage to using a shorter time window. However, with pre-whitening, which is not a linear operation, this no longer holds true. In terms of a red spectral contamination source like MT, first-difference pre-whitening is roughly analogous to a high-pass filter whose corner frequency is a function of the window length. The shorter the time window, the higher the corner. The reason for this is simple. For a given window length T, frequencies below about one-quarter or one-fifth of the lowest frequency that can be derived from the window (i.e. $1/T$) will appear in the time-series as a linear ramp and can be effectively removed by first difference pre-whitening. Shrinking the time window to the length of one source waveform maximizes the effect of the pre-whitener by moving the cut-off frequency close to the fundamental frequency of the source waveform. Thus if one desires long time window TF estimates (e.g. 60 s), it is better to use the shortest time window possible (i.e. one fundamental wavelength long) and average in the frequency domain. When pre-whitening is used, this will yield an improved TF estimate compared to a single, long time window TF estimate.

Eqs (7) and (8) are the first-difference pre-whitening and post-darkening equations, respectively, where lowercase variables x and y are samples in the time domain, uppercase variables X and Y are in the frequency domain, and F is the sampling frequency of the receiver (Shumway & Stoffer 2000, Ch 3).

$$y_j = x_{j+1} - x_j, \tag{7}$$

$$X(f) = \frac{Y(f)}{e^{2\pi i f/F} - 1}. \tag{8}$$

The pre-whitener is applied in the time domain, the data are Fourier transformed into the frequency domain, then the post-darkener is applied to remove the amplitude and frequency effects of the filter. First differencing is not as aggressive as some pre-whiteners such as auto-regressive filters; however, it has the advantage that the post-darkening step is analytical and complete; no residual amplitude or phase distortions remain on the data after post-darkening.

In the Scarborough survey data shown in Fig. 5, we used waveform D with a fundamental frequency of 0.25 Hz. To derive the CSEM data at each receiver, we used an FFT with a 4 s window (i.e. one waveform in length). Each time-series window was pre-whitened by first differencing to remove the effects of long-period MT noise. After transformation into the frequency domain, the data were post-darkened to remove the phase and amplitude effects of the pre-whitener. The TF estimates from the 4 s windows were then averaged to yield TF estimates for 60 s windows. With first differencing, we observe a factor of two reduction in the noise floor compared to without differencing. Since we are using a short time window, polynomial noise reduction such as described by Pankratov & Geraskin (2010) is not necessary. Indeed, in a short time window, polynomial noise reduction could have the undesirable effect of partially removing the CSEM signal.

Another practical benefit of the use of the average of short time windows is that it allows derivation of a variance estimate for each stacked TF datum. For each set of data to be averaged, we calculate the variance of the mean using the complex amplitudes. To do this, we use the Bienaymé formula that states that the variance of the mean is the mean of the variances, where the variance of each datum is assumed to be equal (Loeve 1978). When calculating this value, it is important to consider the decay in amplitude with increasing range. As with the case of stacking bias discussed earlier, the linear component of this decay does not bias the use of averages—the average of the amplitudes and the average of the ranges define a point that lies on a linear trend of amplitude with range, and inclusion of the linear part of the decay in our estimation of variance will result in an overestimate. Rather, we remove a linear trend from the data and estimate the variance of the residuals, dividing by the number of data to get the variance in the mean.

Fig. 7 shows 60 s TF amplitude estimates for 0.75 Hz derived in this way. The variance estimates (plotted as standard deviation) are shown by the thin line below the TF data. At close ranges the variance is inflated by the accentuated curvature of the exponentially decaying signal. This is the bias discussed above and modelled in Fig. 6. Because it is relatively small (0.1 per cent of signal amplitude or less), we make no attempt to remove it from the TF estimate. After a kilometre in range, the variance estimate settles to a constant value. Since the data also settle to this value at longer ranges, we take it to be the system noise floor and validation that our variance estimation procedure is correct.

Both the long time window and the average of short time windows are subject to bias from noise contamination of the time-series as discussed earlier. Brief excursions of the variance from the noise

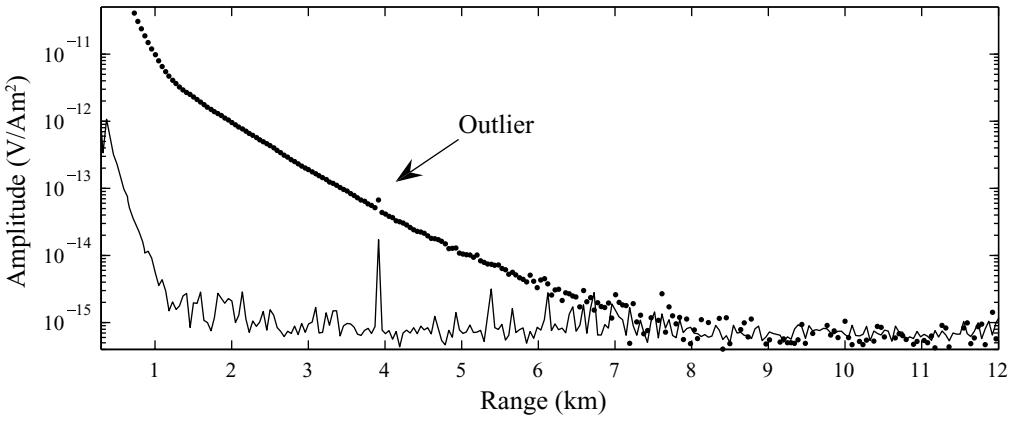

Figure 7. 60 s 0.75 Hz electric-field transfer function amplitude estimates (filled circles) and variance estimates (line; plotted as standard deviation) from a site in the Scarborough survey. TF estimates are each the mean of fifteen 4 s estimates. Variance estimates are calculated using the procedure described in the text. At close range, the variance estimate is high due to bias from the curvature of the exponential decay. After about 1 km range, the variance settles to the noise floor, as verified by the long range TF data. The outlier identified in the plot is discussed in the text and shown in Fig. 8.

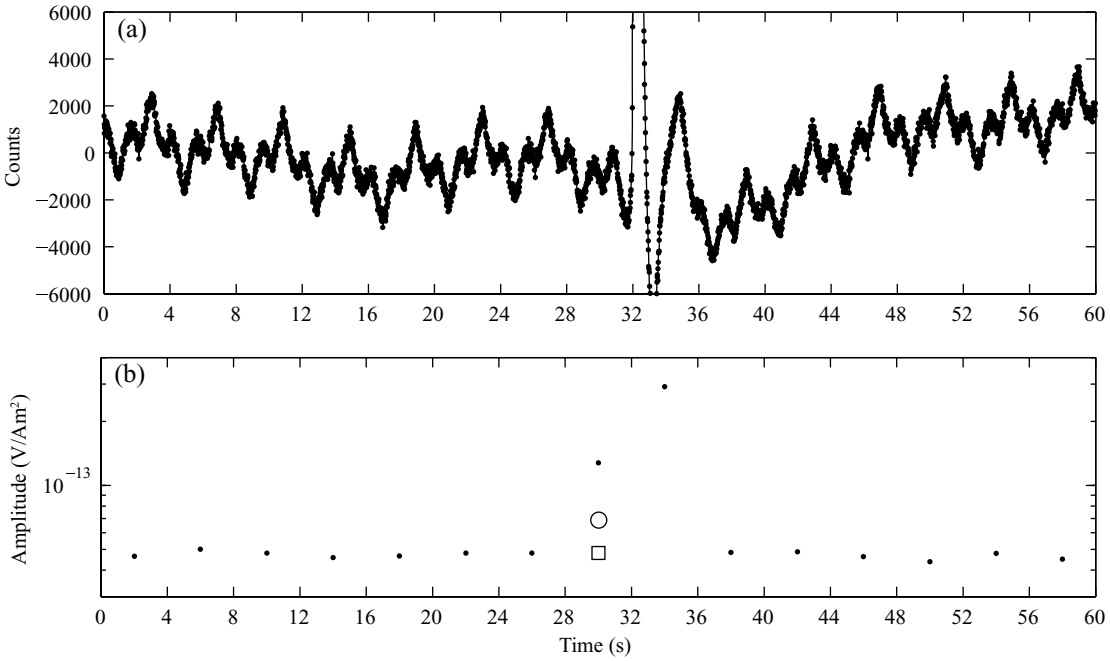

Figure 8. (a) 60 s of time-series from around the outlier shown in Fig. 7 near 4 km range. The spike in the time-series between 28 and 36 s is from the activation of an acoustic transponder. (b) The 4 s TF amplitude estimates for 0.75 Hz derived from the time-series. Note the outlier values caused by the time-series spike. The arithmetic mean of these data (circle) is ∼40 per cent higher than the median (square), which is more robust.

floor in Fig. 7 indicate points which are biased by noise transients in the time-series. An advantage of using the short time window is that the averaging can be replaced with any of a variety of robust stacking techniques. Transient defects in the time-series can be common in CSEM data and usually are of very short duration—less than one waveform in length. TF estimates for time windows containing these defects may be abnormally high and consequently can bias the statistical average, which is notoriously sensitive to outliers. In Fig. 8 we show 60 s of time-series from the Scarborough survey with a short duration defect caused by activation of the receiver's acoustic transponder. Below the time-series are the TF estimates for 0.75 Hz showing the outlier points caused by the electric field spike. The circle shows the average of the estimates and the square shows the median, which is less sensitive to outliers. The expected value should lie near and above the 4 s data, which are slightly concave upwards because of exponential decay of the electric field. As expected, the median provides a better TF estimate than the mean, which in this example is biased ∼40 per cent. For noisier data, more complicated methods than the median may be used to identify outliers and exclude them from the stacking and variance calculations, thus also improving the variance estimation procedure.

It is important to note that the estimate from a long time window is identically sensitive to outliers, since the estimate from a long time window is identical to the average of estimates of short time windows. Had we used 60 s of time-series to produce the TF estimate, we would have derived a biased estimate, which would have to be discarded. In our procedure, in which we take advantage of the compactness of the waveform to derive short-time TF estimates, the effect of outliers can be reduced or eliminated from the long-time TF estimates, thus increasing the amount and quality of available data.

6 CONCLUSIONS

Binary and ternary waveform design can be improved by recognizing that the class of doubly symmetric waveforms has special properties: they are compact, have controlled phase, are never polarizing, and can be described by a close-form solution which makes searching the entire class tractable on a standard computer. We have searched the class for a waveform in which two of the middle harmonics (third and seventh) are maximized and shown with data from a survey off the coast of Australia that the resulting waveform is a reasonable choice for collecting multi-frequency data in hydrocarbon-related CSEM surveys.

The use of compact waveforms allows for more robust statistical methods to be introduced into CSEM time-series processing. Using short, waveform-length, time windows and a simple first-difference pre-whitener lessens spectral contamination from MT or other low frequency noise. The detailed data may then be robustly stacked to the more typical 60+ s time windows, while reducing bias from time-series transients. Variance estimates may also be derived to accurately characterize the instrument noise floor and, at close ranges, the curvature bias from the rapid exponential decay.

ACKNOWLEDGMENTS

The authors acknowledge funding support from BHP Billiton and the Seafloor Electromagnetic Methods Consortium at the Scripps Institution of Oceanography. We thank David Jabson for helpful discussion, and Rune Mittet and an anonymous reviewer for many useful suggestions. We thank Phillip K. Dick for inspiring the name of our waveform.

REFERENCES

Behrens, J.P., 2005. The detection of electrical anisotropy in 35 Ma pacific lithosphere, *PhD thesis*, University of California.

Bendat, J.S. & Piersol, A.G., 2000. *Random Data: Analysis and Measurement Procedures,* 3rd edn, Wiley, New York.

Constable, S. & Cox, C.S., 1996. Marine controlled-source electromagnetic sounding. Part 2: the PEGASUS experiment, *J. geophys. Res.,* **101,** 5519–5530, doi:10.1029/95JB03738

Constable, S. & Srnka, L.J., 2007. An introduction to marine controlled-source electromagnetic methods for hydrocarbon exploration, *Geophysics,* **72,** WA3–WA12, doi:10.1190/1.2432483

Cox, C.S., Constable, S.C., Chave, A.D. & Webb, S.C., 1986. Controlled-source ElectroMagnetic sounding of the oceanic lithosphere, *Nature,* **320,** 52–54, doi:10.1038/320052a0

Edwards, N., 2005. Marine controlled source electromagnetics: principles, methodologies, future commercial applications, *Surv. Geophys.,* **26,** 675–700. doi:10.1007/s10712-005-1830-3

Eidesmo, T., Ellingsrud, S., MacGregor, L.M., Constable, S., Sinha, M.C., Johansen, S., Kong, F.N. & Westerdahl, H., 2002. Sea Bed Logging (SBL), a new method for remote and direct identification of hydrocarbon filled layers in deepwater areas, *First Break,* **20,** 144–152.

Ellingsrud, S., Eidesmo, T., Johansen, S., Sinha, M.C., MacGregor, L.M. & Constable, S., 2002. Remote sensing of hydrocarbon layers by seabed logging (SBL): results from a cruise offshore Angola, *Leading Edge,* **21,** 972–982, doi:10.1190/1.1518433

Key, K., 2009. 1D inversion of multicomponent, multifrequency marine CSEM data: methodology and synthetic studies for resolving thin resistive layers, *Geophysics,* **74,** F9–F20, doi:10.1190/1.3058434

Loeve, M., 1978. *Probability Theory,* 4th edn, Vol. 45, Springer-Verlag, New York.

Loseth, L.O., Pedersen, H.M., Ursin, B., Amundsen, L. & Ellingsrud, S., 2006. Low-frequency electromagnetic fields in applied geophysics: waves or diffusion? *Geophysics,* **71,** W29–W40, doi:10.1190/1.2208275

Lu, X. & Srnka, L.J., 2005. Logarithmic spectrum transmitter waveform for controlled-source electromagnetic surveying: U. S. Patent WO 2005/117326A2.

MacGregor, L., Sinha, M. & Constable, S., 2001. Electrical resistivity structure of the Valu Fa Ridge, Lau Basin, from marine controlled-source electromagnetic sounding, *Geophys. J. Int.,* **146,** 217–236, doi:10.1046/j.1365-246X.2001.00440.x

McFadden, P.L. & Constable, S.C., 1983. The estimation and removal of a linear drift from stacked data, *J. Geophys.-Z. Geophysik,* **53,** 52–58.

Mittet, R. & Schaug-Pettersen, T., 2008. Shaping optimal transmitter waveforms for marine CSEM surveys, *Geophysics,* **73,** F97–F104, doi:10.1190/1.2898410

Myer, D., Constable, S. & Key, K., 2010. A marine EM survey of the Scarborough gas field, Northwest Shelf of Australia, *First Break,* **28,** 77–82.

Pankratov, O.V. & Geraskin, A.I., 2010. On processing of controlled source electromagnetic (CSEM) data, *Geologica Acta,* **8,** 31–49.

Shumway, R.H. & Stoffer, D.S., 2000. *Time Series Analysis and its Applications,* 1st edn, Springer-Verlag, New York, doi:10.1007/978-1-4419-7865-3

Sinha, M.C., Patel, P.D., Unsworth, M.J., Owen, T.R.E. & Maccormack, M.R.G., 1990. An active source electromagnetic sounding system for marine use, *Mar. Geophys. Res.,* **12,** 59–68, doi:10.1007/BF00310563

Ward, S.H. & Hohmann, G.W., 1987. Electromagnetic theory for geophysical applications, in *Electromagnetic Methods in Applied Geophysics,* Vol. 1, ed. Nabighian, M.N., Soc. Exploration Geophysicists, Tulsa, OK.

Weitemeyer, K. & Constable, S., 2010. Mapping shallow geology and gas hydrate with marine CSEM surveys, *First Break,* **28,** 97–102.

Weitemeyer, K.A., Constable, S.C., Key, K.W. & Behrens, J.P., 2006. First results from a marine controlled-source electromagnetic survey to detect gas hydrates offshore Oregon, *Geophys. Res. Lett.,* **33,** doi:10.1029/2005gl024896